Fe-modified sporopollenin as a composite biosorbent for the removal of Pb^{2+} from aqueous solutions

Murat Şener[a], Berkant Kayan[a,*], Sema Akay[a], Belgin Gözmen[b], Dimitrios Kalderis[c,*]

[a]Faculty of Arts and Science, Department of Chemistry, Aksaray University, Aksaray, Turkey, email: murat_kan77@hotmail.com
(M. Şener), Tel. +90 3822882693; Fax: +90 2428248231; emails: berkantkayan@gmail.com (B. Kayan),
sema.akay7@gmail.com (S. Akay)
[b]Faculty of Arts and Science, Department of Chemistry, Mersin University, Ciftlikkoy Campus, Mersin, Turkey,
email: bgozmen@gmail.com
[c]Department of Environmental and Natural Resources Engineering, School of Applied Sciences, Technological and Educational
Institute of Crete, Chania, Crete, Greece, Tel. +30 2821023017; Fax: +30 2821023003; email: dkalderis@chania.teicrete.gr

ABSTRACT

The role of Fe-modified sporopollenin (Fe-Sp) biomass in Pb^{2+} removal from aqueous solutions was investigated by batch biosorption technique. The prepared biosorbent was characterized by scanning electron microscopy, energy-dispersive X-ray spectrometry, and Fourier transform infrared spectroscopy. The influence of pH, contact time, biosorbent dose, and initial concentration on biosorption process were optimized by using a four factor Box–Behnken design combined with response surface methodology. The results indicated a positive adsorption behavior of Fe-Sp and a strong pH dependency of the process. The optimum predicted parameters were determined as follows: biosorbent dosage 0.5 g, pH of 6.75, contact time 104 min, and initial Pb^{2+} concentration of 25.42 ppm. The Freundlich isotherm model provided a better fit ($R^2 = 0.994$) for the experimental data, indicating biosorption on a heterogeneous surface. Maximum biosorption capacity (q_{max}) was 22.72 mg g^{-1} as indicated by the Langmuir isotherm. Kinetically, the adsorption process followed a pseudo-second-order model, indicating that chemisorption was the rate-limiting step.

Keywords: Fe-modified sporopollenin; Biosorption; Response surface methodology; Lead removal

1. Introduction

Several industries worldwide produce wastewaters with elevated concentrations of heavy metals. If these are left untreated, they pose a significant environmental threat to receptive bodies. The toxicity and health risks of heavy metals such as lead, chromium, cadmium, mercury, and arsenic have been well estab-

lished [1]. Lead has been one of the most widely used metals since the ancient times. It exhibits a range of favorable properties for many applications, such as in pigments and paints, storage batteries, vinyl products, ammunition, and radiation shielding materials. Exposure to lead may arise from contact with contaminated water and soil, as well as inhalation of gaseous emissions from lead-containing fuels. The World Health Organization has established a drinking water limit of

*Corresponding authors.

$10 \ \mu g \ L^{-1}$ for lead. Flora et al. [2] provide a comprehensive update on the effects of lead poisoning in the human body and the latest available therapies.

Various technologies have been tested for the removal of lead and other heavy metals from wastewater. Chemical precipitation, ion exchange, electrochemical methods, adsorption on activated carbon, and membrane filtration have received most of the scientific attention [3,4]. The mechanisms, advantages, and disadvantages for each one of these, are thoroughly reviewed by Fu and Wang [5]. The effectiveness of each technology depends on a number of parameters, therefore determining the optimum removal conditions for wastewaters containing several heavy metals, can be complicated.

Lately, biosorption has been considered as an efficient alternative to conventional treatment of heavy metal wastewaters. Biosorption is based on the use of agricultural waste and other types of biomass for the removal of heavy metals from aqueous solutions. Nowadays, valorization of agricultural waste is a critical component for sustainable environmental protection in many countries worldwide. The main advantage of biosorption is the relatively high sorption capacity, low cost, and availability of the biomass. Common biosorbents include rice and other husks, fruit peels, nut shells, flower petals, coffee waste, and chitosan [6–8]. Heavy metal bio-sorption is a combination of precipitation, ion exchange, surface interactions, diffusion, and chelation phenomena, all of which are pH-dependent to a certain degree. Chemical of physical modification is often used to improve the overall sorption capacity of the biomass [9,10].

One type of biomass that has recently attracted attention for heavy metal removal from water is sporopollenin. Sporopollenin is one of the main constituents of the tough external walls of plant spores and pollen grains. It is chemically very stable and usually well preserved in soils and sediments. Due to this resistance to physical, chemical, and biological degradation, the exact structure of sporopollenin is still unknown. It is considered to be a highly cross-linked organic polymer with long aliphatic chains, conjugated phenols, hydroxyls, ethers, methyls, and carboxylic acids [11,12].

The use of sporopollenin as an adsorbent has certain advantages, mainly its significant sorption properties toward heavy metals, low cost, and natural abundance. To date, it has been successfully used in cases of chromium, lead, cobalt, copper, nickel, zinc, and cadmium contaminated wastewaters [13–17]. Additionally, it has been proven effective in removing excess concentrations of boron [18], ruthenium [19], and vanadium [20] from aqueous solutions. The sorption and structural properties of sporopollenin can be further improved through surface modification; however, this area of research is largely unstudied and the published literature is scarce [14,21,22].

In many cases of material surface modification, this includes the formation of Fe-modified composites with natural or polymeric materials. These composites can be prepared through various techniques and used in a wide range of applications, such as sensors, magnetic data storage, medical care, colorimetric assays, and wastewater treatment [23–32].

As reviewed by Sivashankar et al. [33], magnetically modified biosorbents exhibit promising adsorption capacity toward mixed wastewaters (both with heavy metals and organics). The main reason for preparing magnetic (or nano-magnetic) composites is that the magnetite particles often have a much higher surface area compared to that of the raw biomass, therefore the adsorption behavior of the composite is considerably improved [34,35]. Additionally, the traditional methods of separation after adsorption–filtration, sedimentation, and centrifugation—are often inefficient and uneconomical. Magnetic carriers serve as supporting materials for adsorbents. The contaminant-loaded composite can be easily separated and recovered from the aqueous solution [36,37].

Both Yavuz et al. [38] and Mahmoud et al. [39] studied the adsorption of Hg^{2+} on magnetically modified composites based on yeast. The optimum biosorption capacities they found were comparable, 76.2 and $64 \ mg \ g^{-1}$ at 25℃, respectively. Both groups pointed out that pH was the determining factor for the process. A yeast-coated magnetic composite was also used by Abdel-Fattah et al. [40] for the removal of Cr^{+3} and Cr^{+6} from aqueous solutions. They achieved high removal percentages ranging between 90 and 100% for both species. Using iron oxides particles, Wang et al. [41] modified wheat bran and determined the removal efficiency of uranium from aqueous solutions. As in the case of mercury, pH was also the determining factor for the biosorption of uranium. Kamboh and Yilmaz [18] converted sporopollenin to magnetic sporopollenin by impregnation in iron salts. Then, they grafted the magnetic biosorbent to *N*-methylglucamine calix [4] arene, in order to form a novel adsorbent material with improved thermal, chemical, and physical stability. The new bio-composite showed a positive adsorption behavior and was successful in removing boron from aqueous solutions (adsorption capacity $12.3 \ mg \ g^{-1}$ at 25℃).

To investigate further the properties of Fe-modified sporopollenin (Fe-Sp) and add new knowledge to this area of research, it was decided to study the behavior of this bio-composite toward adsorption of Pb^{2+} from aqueous solutions. The objectives of this study are: (1)

synthesis of a novel Fe-modified biosorbent from sporopollenin biomass impregnated with Fe_3O_4 particles and characterization with respect to scanning electron microscopy (SEM), Fourier-transform infrared spectroscopy (FTIR), and energy dispersive X-ray (EDX) analysis, (2) to study the Pb^{2+} removal from aqueous solution and apply a four-factor Box–Behnken experimental design combined with response surface methodology (RSM) for determining the optimum biosorption conditions, (3) to examine the effects of four independent variables (biosorbent dosage, pH, contact time, and initial Pb^{2+} concentration) and their interactions on the biosorption capacity, (4) application of the Langmuir and Freundlich isotherm models to provide a better understanding of sorbate and sorbent interactions, and (5) kinetic adsorption investigation based on the pseudo-first-order, pseudo-second-order, and the intra-particle diffusion models.

RSM is a combination of mathematical and statistical techniques used to study the effect of several variables influencing the responses by varying them simultaneously and carrying out limited number of experiments. The validity of the method has been well established for a wide range of adsorbents and adsorption experimental designs [42–44]. However, there is no information available in the literature regarding the optimization of Pb^{2+} biosorption on Fe-Sp.

2. Materials and methods

2.1. Materials

L. clavatum spores (sporopollenin) of 20 μm particle size were obtained from Sigma-Aldrich (Steinheim, Germany). Typical elemental analysis and surface area for this type of sporopollenin is 62.1% C, 7.3% H, 0.1% N, and ~4 $m^2\,g^{-1}$, respectively [12]. All reagents used were of analytical grade and obtained from Merck (Germany). Ultra-pure water (18.2 MΩ cm^{-1}) was used for preparation of all solutions (MilliPore Milli-Q Gradient water purification system). Analytical grade $PbNO_3$ was used to prepare a stock solution of 1,000 mg L^{-1} concentration. Each sample solution was prepared at the required concentrations by serial dilution of the stock solution with ultra-pure water. The pH was adjusted by addition of either 0.1 M HCl or 0.1 M NaOH and the pH value was monitored with a Hanna HI 2211 model digital pH-meter (USA).

2.2. Preparation of Fe-modified sporopollenin (Fe-Sp)

Fe-Sp was prepared through chemical precipitation of iron oxide particles on the sporopollenin surface, in a basic environment. The process is reported in detail in Kamboh and Yilmaz [18] and is briefly described below. $FeCl_3\cdot6H_2O$ (13.32 g), $FeCl_2\cdot4H_2O$ (19.88 g), HCl (5 mL–5 M), ultra-pure water (40 mL), and ethanol (5 mL) were mixed in a 100 mL flask followed by heating to 40°C until complete dissolution of the salts. Sporopollenin (1 g) was then added in 30 mL of this solution and stirred for 2 h at room temperature. The suspension was then filtered, washed with water, and poured into 10 mL of 1 M ammonia solution. After a further 2 h of stirring, the Fe-modified biosorbent (with Fe_3O_4 particles embedded) was collected by magnet, washed to neutral pH with water, dried in vacuum at 50°C for 24 h, and finally stored for further use (Fig. 1). Practically the same procedure has been used in the past to prepare magnetic chitosan [45,46] and other magnetic biosorbents [33,40].

2.3. Characterization of the Fe-modified composite and analytical methods

Fe-Sp was morphologically characterized in a Zeiss/Supra 55 (Germany) high-resolution scanning electron microscope. As soon as the biosorption process was completed, the biosorbents were recovered from solution by centrifugation. The residual Pb^{2+} concentration was measured in a flame atomic absorption spectrometer (Thermo Scientific ICE 3400-USA) with an air-acetylene flame and a hollow cathode lamp at a wavelength of 217.0 nm. The infra-red (IR) spectra of the Fe-Sp and metal-loaded Fe-Sp samples (as KBr pellets) were recorded by using an IR spectrophotometer Perkin–Elmer FT-IR (USA). EDX spectroscopy analysis was done using a Quantax instrument (Bruker, USA).

The surface chemistry of Fe-Sp during adsorption was investigated further through the determination of the pH point of zero charge (pH_{pzc}). At pH values above the zero point charge, the surface of the sorbent has a net negative or anionic charge, and the surface
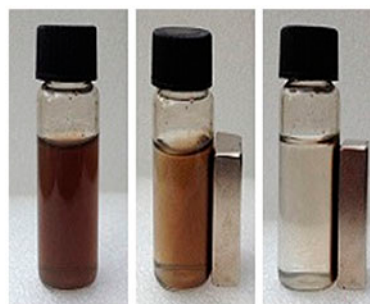

Fig. 1. Preparation of Fe-modified sporopollenin (Fe-Sp).

would promote cation attraction, and cation exchange reactions. At pH values below the zero point charge, the surface has a net positive charge, and the surface will attract anions, and participate in anion exchange reactions. The pH_{pzc} was determined using the methodology described in Newcombe et al. [47].

2.4. Pb^{2+} biosorption experiments

The biosorption experiments were performed according to the procedure reported at Şener et al. [16]. Pb^{2+} solutions of concentrations in the range of 10–60 mg L^{-1} were used and the removal percentage was calculated according to the following formula:

$$Removal\ (\%) = \frac{C_0 - C_e}{C_0} \times 100 \tag{1}$$

where C_0 and C_e are the initial and equilibrium concentrations of metal in mg L^{-1}, respectively.

2.5 Biosorption kinetics experiments

The kinetics experiments were performed in essentially the same manner as the batch biosorption experiments described above. For this purpose, 0.5 g of Fe-Sp were added to each of 60 mg L^{-1} Pb solutions. The solutions were then stirred (150 rpm) at room temperature (25°C) for contact times ranging from 10 to 120 min. At the end of each contact time, the solution was filtered and the filtrate was stored for metal analysis. The experimentally recorded sorption per unit weight of solid (q_t) was calculated as follows:

$$q_t = \frac{V(C_0 - C_e)}{m} \tag{2}$$

where V is the volume of the metal solution, C_0 and C_e are the initial and equilibrium concentrations of metal, respectively, and m is the dry weight of the biosorbent. All kinetic experiments were performed in triplicate to ensure reproducibility and the mean values were used for the calculations.

2.6. Box–Behnken design and biosorption optimization

The statistical software Design Expert v.9.0.4 (Stat-Ease Inc., Germany) was used for the experimental design, analysis, and optimization. Two of the most well established quadratic designs are the central composite design (CCD) and Box–Behnken design (BBD). When it comes to investigating four variables, BBD is preferable to CCD because of the fewer run number required to reach 95% confidence level. This has been the design of choice for optimizing heavy metal removal from aqueous solutions in the past [48–52].

This design was also used to study the response pattern and determine the optimum conditions for maximum Pb^{2+} biosorption by Fe-Sp. Biosorbent dose (X_1), pH (X_2), contact time (X_3), and initial Pb^{2+} concentration (X_4) were the four independent variables. The removal percentage was considered as the dependent variable or response (Y). For the statistical calculations, BBD uses the following equation:

$$X_i = \frac{X_i - X_0}{\Delta X_i} \tag{3}$$

where X_i, X_0 are the real values of the independent variable and the independent variable on the center point, respectively, and ΔX_i is the step change value. The experimental range and levels (–1, 0, +1) of independent variables are given in Table 1. BBD resulted in 29 experiments (Table 2) according to the following equation:

$$N = 2k(k-1) + C_0 \tag{4}$$

where k is number of factors, and C_0 is the number of central point [53]. One more run was performed (#30–verification run) to compare the experimental biosorption % to the one predicted by the BBD at the optimum conditions.

The experimental results were analyzed using Design Expert v.9.0.4 and a regression model was proposed. In the optimization process, the responses can be simply related to the chosen factors by linear or quadratic models. A quadratic model, which also includes the linear model, is given below as Eq. (5):

Table 1
Experimental range and levels of the independent variables

| Variables | Factor | Range and level | | |
		–1	0	+1
Biosorbent dose (g)	X_1	0.1	0.3	0.5
pH	X_2	2.0	5.0	8.0
Contact time (min)	X_3	10	110	210
Initial Pb^{2+} concentration (ppm)	X_4	10	35	60

Table 2
Box–Behnken design experiments and experimental results

Run number	Experimental design				Experimental Y Biosorption (%)	Predicted Y Biosorption (%) (% error)
	X_1 B. dose	X_2 pH	X_3 C. Time	X_4 C_{Pb}		
1	0.1	2.0	110	35	13.0	13.13 (1)
2	0.5	2.0	110	35	16.8	20.53 (22.2)
3	0.1	8.0	110	35	74.0	72.08 (2.6)
4	0.5	8.0	110	35	91.0	92.68 (1.8)
5	0.3	5.0	10	10	78.0	85.33 (9.4)
6	0.3	5.0	210	10	97.0	97.15 (0.15)
7	0.3	5.0	10	60	64.0	65.66 (2.6)
8	0.3	5.0	210	60	84.0	78.48 (6.6)
9	0.1	5.0	110	10	87.0	81.20 (6.7)
10	0.5	5.0	110	10	95.0	92.20 (2.9)
11	0.1	5.0	110	60	58.0	59.03 (1.8)
12	0.5	5.0	110	60	72.0	76.03 (5.6)
13	0.3	2.0	10	35	18.0	18.23 (1.3)
14	0.3	8.0	10	35	81.0	77.73 (4)
15	0.3	2.0	210	35	23.0	24.50 (6.5)
16	0.3	8.0	210	35	98.1	96.10 (2)
17	0.1	5.0	10	35	72.0	72.32 (0.44)
18	0.5	5.0	10	35	93.2	86.92 (6.8)
19	0.1	5.0	210	35	79.0	85.24 (7.9)
20	0.5	5.0	210	35	99.0	98.64 (0.36)
21	0.3	2.0	110	10	15.0	12.79 (14.7)
22	0.3	8.0	110	10	94.0	97.34 (3.5)
23	0.3	2.0	110	60	16.0	12.62 (21.1)
24	0.3	8.0	110	60	57.0	59.17 (3.8)
25	0.3	5.0	110	35	63.0	64.10 (1.8)
26	0.3	5.0	110	35	64.0	64.20 (0.3)
27	0.3	5.0	110	35	64.0	64.20 (0.3)
28	0.3	5.0	110	35	65.0	64.20 (1.2)
29	0.3	5.0	110	35	65.0	64.20 (1.2)
30[a]	0.5	6.75	104	25.4	98.8	99.9 ± 4.6

[a]Verification run performed at the optimum conditions predicted by the Box–Behnken design.

$$
\begin{aligned}
Y = {}& \beta_0 + \beta_1 X_1 + \beta_2 X_2 + \beta_3 X_3 + \beta_4 X_4 + \beta_{12} X_1 X_2 \\
& + \beta_{13} X_1 X_3 + \beta_{14} X_1 X_4 + \beta_{23} X_2 X_3 + \beta_{24} X_2 X_4 \\
& + \beta_{34} X_3 X_4 + \beta_{11} X_1^2 + \beta_{22} X_2^2 + \beta_{33} X_3^2 + \beta_{44} X_4^2
\end{aligned} \tag{5}
$$

where Y is the predicted response, X_i indicate the independent variables, β_0, β_i, β_{ii}, and β_{ij} are the constant coefficient, the linear coefficient, the quadratic coefficient, and the interaction coefficient, respectively.

The adequacy of the proposed model was evaluated using the diagnostic checking tests provided by analysis of variance (ANOVA). Determination of R^2 coefficient and adjusted R^2 coefficient indicate the extent to which the experimental values fit the polynomial model. Additionally, the R^2 values are a measure of how the variability in the observed response values can be clarified by experimental factors and their interactions [48,54–56]. The impact and significance of each term in the regression Eq. (5) was evaluated by analysis of variance.

3. Result and discussion

3.1. Characterization of biosorbent

3.1.1. Fourier-transform infrared spectroscopy

The FTIR spectra of sporopollenin, Fe-Sp and Fe-Sp with Pb sorbed are presented in Fig. 2. A broad band ranging from 3,200–3,400 cm^{-1} can be observed due to the presence of hydroxyl groups (–OH). The peaks at 2,923 and 2,854 cm^{-1} were due to aromatic and methylene C–H stretching vibrations, respectively. The peak shown at 1,517 was due to the C=C stretching vibrations of the aromatic rings and the one at 1,710 cm^{-1}
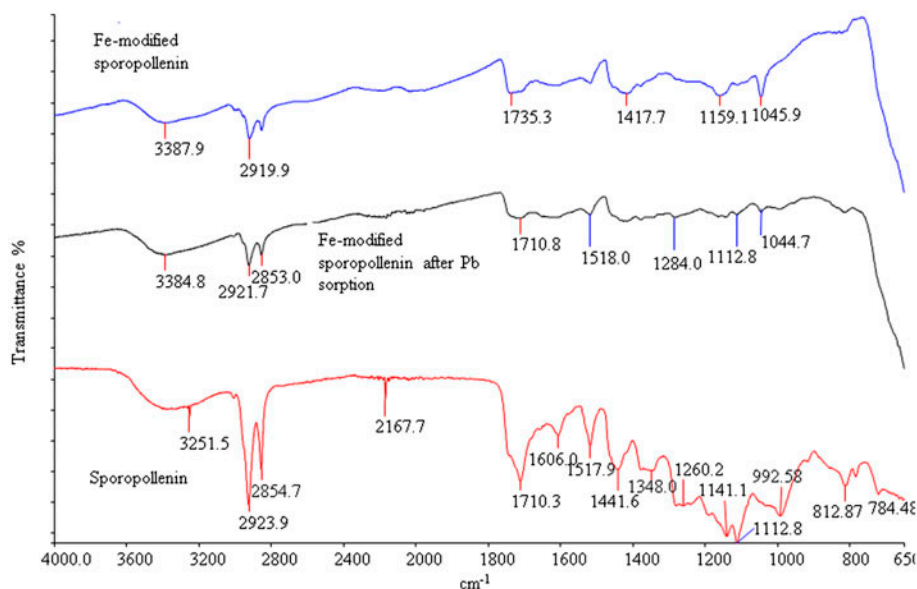
Fig. 2. FT-IR spectra of sporopollenin, Fe-Sp and Fe-Sp with Pb sorbed.

was due to the C=O stretching vibration of an ester linkage. The peaks at 1,141 and 1,112 cm^{-1} were due to the C–O ester linkage and the band 650–784 cm^{-1} was due to the Fe–O bond deformations, which confirms the formation of Fe$_3$O$_4$ particles [18,57,58]. Comparing the FTIR spectra of Fe-Sp and Fe-Sp with Pb sorbed, the peaks at 1,159.1 and 1,045.9 (C–O ester linkage) appear reduced in the latter. This suggests that such ionizable functional group on the adsorbent surface is able to bind with the metal ion.

The assignment of a specific wave number to a given functional group was not possible in all cases, because the absorption bands of various functional groups overlap and shift, depending on their molecular structure and environment. Shifts in absorption positions can be caused by the factors such as intra-molecular and intermolecular hydrogen bonding, inductive effect, steric effects, and degrees of conjugation.

3.1.2. Surface morphology analysis

SEM is known as one of the most widely used surface diagnostic tools. The SEM images (Fig. 3(a) and (b)) revealed that Fe-Sp consists of a uniform interconnected pore structure (in hexagonal shape), in the form of a round microcapsule with a continuous surface. The surface micrographs showed a distinct roughness pattern due to the iron oxide clusters deposited (non-uniformly) inside the pores and on the pore walls. The average size of Fe-Sp particles is within the 32–40 μm range and the pore diameter

varies between 4 and 6 μm. It can be seen from Fig. 3(b), that the Fe$_3$O$_4$ cluster sizes vary widely, ranging from tenths to hundreds of nanometers. The differences between Fe-modified and pure sporopollenin can be seen in Fig. 3(b) and (c). Treatment with FeCl$_2$ and FeCl$_3$ did not change the morphology or size of sporopollenin. Each spore remained hollow and approximately 25 mm in diameter with a hemispherical cap ending in a trilete structure on the underside. This conclusion is also supported by the findings of Archibald et al. [12]. Their study attempted to elucidate the Fe-sporopollenin interactions, using X-ray absorption spectroscopy. They concluded that when FeCl$_2$ solutions were used, there are specific interactions with the sporopollenin surface groups, potentially including the interior as well as the exterior of the spores. If only FeCl$_3$ is used in the precipitation stage, sporopollenin spores just become coated with ferric oxyhydroxide (FeOOH). Additionally, Archibald et al. observed much higher iron loadings when FeCl$_2$ was used, compared to FeCl$_3$. For these reasons, it is necessary to use both salts during the co-precipitation stage. Therefore, since a mixture of both salts was used in this study, the iron loading is expected to occur in the interior as well as a coating on the spore walls. This observation is well supported by Fig. 3(b).

3.1.3. EDX analysis

The EDX was employed to study the elements on the biosorbent surface. In this technique, the sample is
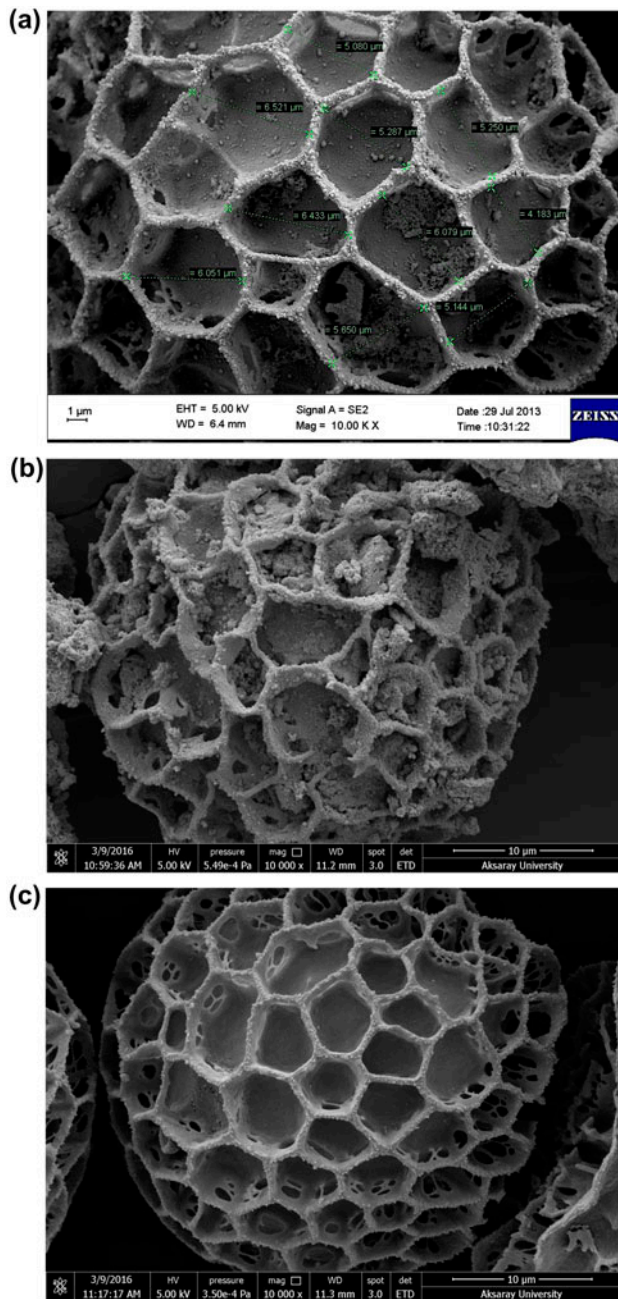
Fig. 3. SEM images of Fe-Sp (a-b) and pure sporopollenin (c).

excited by a highly focused, high-energy primary electron beam and the X-rays are emitted from the sample. In order to confirm the presence of Pb^{2+} in the Fe-Sp, EDX spectra before and after biosorption were recorded (Fig. 4(a) and (b)). In Fig. 4(a), the Fe peaks are at 6.4, 7.06, and 0.705 keV. Oxygen and carbon is observed at 0.277–0.525 keV, respectively. Furthermore, in Fig. 4(b), the Pb peak can be seen at

2.5 keV. Fig. 4(c) shows the distribution of the Fe atoms on sporopollenin.

3.2. Biosorption optimization using BBD

The independent variables and their levels for BBD given in coded and actual values with the responses of each experimental run, are shown in Tables 1 and 2.

3.2.1. Multiple regression modeling

The data in Table 2 were analyzed with Design Expert software v.9.0.4. Based on the results, the following fitted regression model was developed as an empirical relationship between the biosorption percent (response, Y) and independent variables (adsorbent dosage, X_1; pH, X_2; contact time, X_3; and initial Pb^{2+} concentration, X_4) and expressed as second-order polynomial Eq. (6):

$$\begin{aligned} Y = {} & \text{Biosorption \%} \\ = {} & 64.20 + 7.00X_1 + 32.77X_2 + 6.16X_3 - 9.58X_4 \\ & + 3.30X_1X_2 - 0.30X_1X_3 + 1.50X_1X_4 + 3.02X_2X_3 \\ & - 9.50X_2X_4 + 0.25X_3X_4 + 8.52X_1^2 - 23.12X_2^2 \\ & + 13.06X_3^2 + 4.40X_4^2 \end{aligned}$$

(6)

This Eq. (6) showed that pH ($\beta_2 = 32.77$) is the crucial factor for biosorption of Pb^{2+} ions on Fe-Sp. When adsorbent dosage ($\beta_1 = 7.00$) and contact time ($\beta_3 = 6.16$) have positive influence on biosorption, initial metal ion concentration ($\beta_4 = -9.58$) affected it negatively.

3.2.2. Analysis of variance

In order to ensure the statistical significance of the quadratic model employed for fitting the experimental data at a 95% confidence level, the model was tested by analysis of variance. The impact and significance of each term of Eq. (6) and the results are presented in Table 3. On the basis of the experimental values, statistical testing was carried out using Fisher's test (F-test). The F-value is used to test the significance of adding new model terms to the existing ones. The p-values (shown in Table 3) were also used to check the significance of each coefficient and display the interaction pattern between the variables. It can be seen from Table 3 that all the linear and quadratic terms were statistically significant ($p < 0.05$) and played an important role in the biosorption of Pb^{2+}.
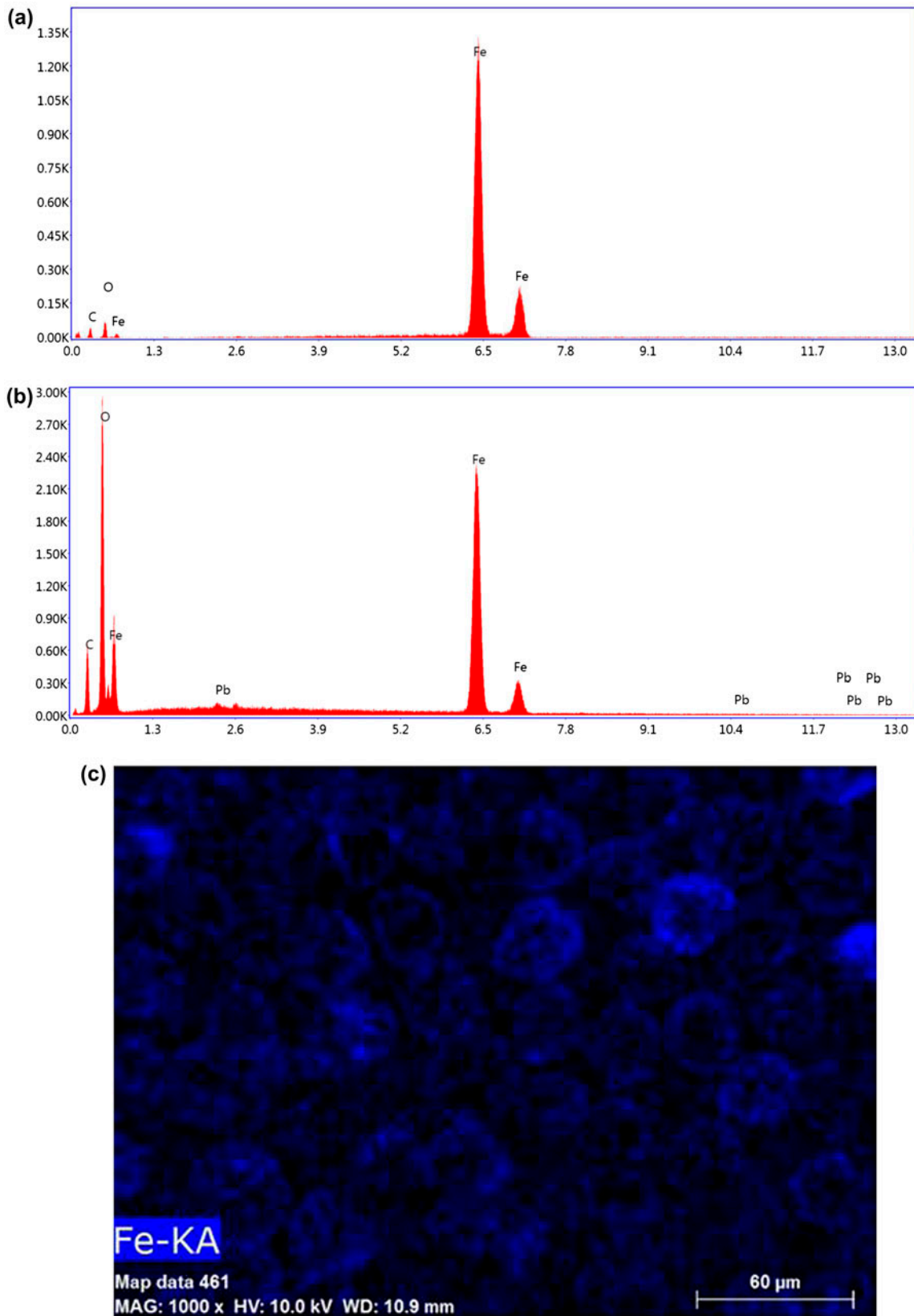
Fig. 4. EDX spectra of Fe-Sp before (a) after (b) biosorption of Pb^{2+}, and elemental mapping (Fe) (c).

Table 3
ANOVA results of the quadratic model for Pb^{2+} biosorption by Fe-modified sporopollenin

Source	Degrees of freedom	Sum of squares	Mean square	F-value	p-value
Model	14	21,853.10	1,560.94	73.64	<0.0001
X_1: Biosorbent (g)	1	588.00	588.00	27.74	0.0001
X_2: pH	1	12,890.41	12,890.41	608.16	<0.0001
X_3: Time (min)	1	455.10	455.10	21.47	0.0004
X_4: İnitial Pb concentration (ppm)	1	1,102.08	1,102.08	52.00	<0.0001
$X_1 \times X_2$	1	43.56	43.56	2.06	0.1736
$X_1 \times X_3$	1	0.36	0.36	0.017	0.8982
$X_1 \times X_4$	1	9.00	9.00	0.42	0.5252
$X_2 \times X_3$	1	36.60	36.60	1.73	0.2099
$X_2 \times X_4$	1	361.00	361.00	17.03	0.0010
$X_3 \times X_4$	1	0.25	0.25	0.012	0.9151
X_1^2	1	470.95	470.95	22.22	0.0003
X_2^2	1	3,466.25	3,466.25	163.54	<0.0001
X_3^2	1	1,106.08	1,106.08	52.18	<0.0001
X_4^2	1	125.34	125.34	5.91	0.0290
Residual	14	296.74	21.20		
Lack of fit	10	293.94	29.39	41.99	0.0013
Pure error	4	2.80	0.70		
Cor. total	28	22,149.84			

Notes: $R^2 = 0.9866$, CV% = 7.04, Adequate precision = 25.97.

The impact each of these terms made may be ranked as follows: X_2: pH > X_4: C_{Pb} > X_1: Biosorbent > X_3: time according to the F-values. When the two most effective terms were related to each other ($X_2 \times X_4$), the combined effect of the terms ($X_1 \times X_3$) and ($X_3 \times X_4$) was negligible. As expected, the quadratic effect of the pH was found to be more the most influential. Overall, it could be said that the most influential biosorption variable was the pH.

The predicting ability of the model was studied using the F-test, p-value, chi-square (X^2), the root mean square error of prediction (RMSEP), the relative error of prediction (RSEP), correlation coefficient (R^2), and adjusted correlation coefficient (R_{adj}^2) [42]. The obtained F-value was 73.64 followed by a very low probability value (p model < 0.0001) which was greater than the critical value of F ($F_{\alpha,df,(n-df+1)} = F_{0.05,14,14} = 2.48$) using $\alpha = 0.05$ (95% significance), confirming the adequacy of the model. If the model is a good predictor of the experimental results, F-value should be greater than the tabulated or critical value. In general, variable terms having probability value below 0.05 at the 95% confidence level, indicates great significance for the corresponding coefficient. A comparison between the predicted and experimental values for biosorption of Pb^{2+} ions is shown in Fig. 5. The correlation coefficients indicate the reliability of the quadratic model. The obtained R^2 and R_{adj}^2 values were 0.9866 and 0.9732, respectively.

The chi-square (X^2), RMSEP and RSEP values were calculated as follows [59,60]:

$$\text{chi-square} = \sum_{i=1}^{N} \frac{\left(Y_{\text{mean},i} - Y_{\text{pred},i}\right)^2}{Y_{\text{pred},i}} \tag{7}$$

$$\text{RMSEP} = \sqrt{\frac{\sum_{i=1}^{N} \left(Y_{\text{pred},i} - Y_{\text{meas},i}\right)^2}{N}} \tag{8}$$

$$\text{RSEP} = \sqrt{\frac{\sum_{i=1}^{N} \left(Y_{\text{pred},i} - Y_{\text{meas},i}\right)^2}{\sum_{i=1}^{N} \left(Y_{\text{meas},i}\right)^2}} \times 100 \tag{9}$$

where $Y_{\text{pred},i}$ and $Y_{\text{meas},i}$ are the model predicted and measured values of the response, Y and N is the number of run. The chi-square value was obtained as 5.26 which was lower than the tabulated value ($X_{0.05}^2 = 23.68$). This result demonstrated that there was no a significant difference between the experimental data and the model response. RMSEP and RSEP values were also calculated as 3.20–4.51%, respectively.

Fig. 5(b) contains a plot of the normal probability of the residuals that should be normally distributed for biosorption percent of Pb^{2+}. The residuals indicate how well the model fulfills the assumptions of the ANOVA where the standardized residuals measure the number of standard deviation (σ) separating the actual and

(a)

Predicted vs. Actual

(b)
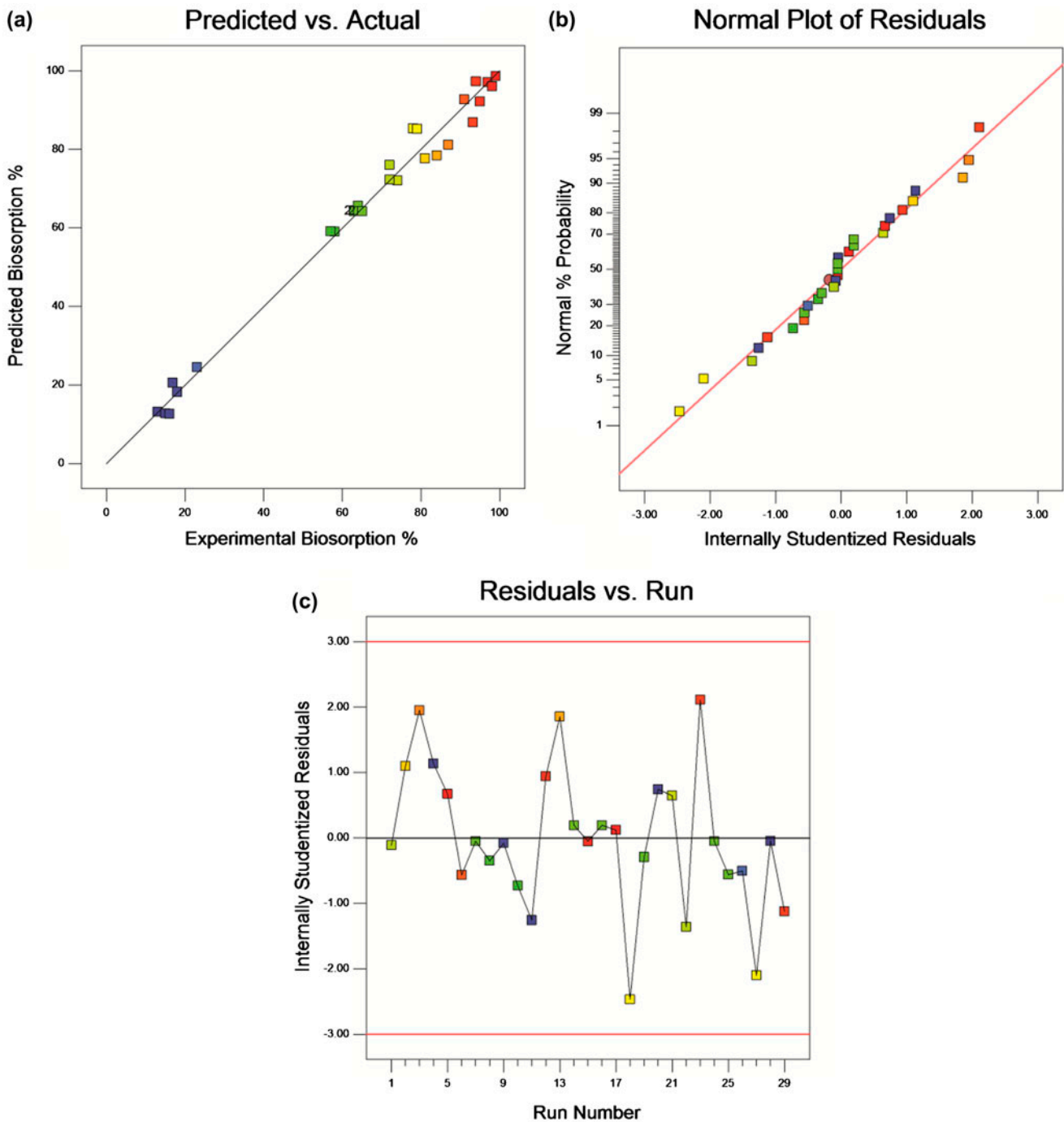
Normal Plot of Residuals

(c)

Residuals vs. Run

Fig. 5. (a) The actual and predicted plot of biosorption % (R^2 = 0.9866, R^2_{adj} = 0.9732), (b) the standardized residual and normal % probability plot of biosorption %, and (c) the standardized residuals plot for biosorption %.

predicted values. Fig. 5(c) discloses that the lurking variable that may have influenced the response during the experiment is the normal plot of the standardized residuals vs. the experimental run number. A random scatter around the center line within the interval of ±3.00 (limits ± 3.00 σ), shows no apparent deviation with the observation order. Otherwise, an observation that is outside of this interval is a potential outlier.

3.2.3. Three-dimensional (3D) response surfaces

The contour plots and the corresponding 3D views provide valuable insight on the influences of the independent variables and their interactions on the dependent variables based on the model equation (Eq. (6)).

3.2.3.1. Interactive effect of biosorbent dosage and initial Pb^{2+} concentration. The interactive effect of the biosorbent dosage and initial Pb^{2+} concentration on the biosorption percent, while holding pH at 6.00 (to avoid potential precipitation of Pb^{2+} at higher pH values) and contact time 120 min is shown in Fig. 6(a). The surface is rather uniform throughout and shows neither sharp increases nor decreases on biosorption as the variables change values. At the lowest biosorbent dosage of 0.1 g, as the initial Pb^{2+} increased, predicted biosorption was decreased from 88 to 74%. Approximately the same pattern was observed at the highest biosorbent dose of 0.5 g. This behavior indicates that at constant pH and contact time, the biosorbent dosage and initial metal concentration were not the dominant parameters of the process.

3.2.3.2. Interactive effect of pH and biosorbent dose. Fig. 6(b) presents the interactive effect of pH and biosorbent dose at constant treatment time and initial Pb^{2+} concentration (20 ppm). Contrary to Fig. 6(a), in this case the dramatic effect of the pH changes can be observed. Regardless of biosorbent dose, it is clear that maximum predicted biosorption was achieved at pH values higher than six. As pH was lowered toward the value of two, the biosorption % falls very steeply. The lower predicted Pb^{2+} removal at this end of the pH scale may be explained by the H^+-saturated Fe-Sp surface. Although the chemical structure of sporopollenin has not been fully revealed, it is well known that it contains hydroxyl and carboxylic moieties [12]. These moieties result in an overall negative charge at the sorbent's surface. In solution, high H^+ concentrations mean that the sporopollenin surface becomes more positively charged, thus reducing the attraction between the biosorbent and metal cations. Practically, H^+ compete with Pb^{2+} for occupancy of the surface active sites [61,62]. As pH increases, more negatively charged surface becomes available which promotes greater metal uptake, and therefore metal sorption tends to increase significantly [21].

Increasing the biosorbent dosage at constant pH had practically no effect on biosorption. One would expect that as the biosorbent dosage increased, so would the "active sites" available for sorption. This was not predicted by the model, indicating that the role of pH was so determining that did not allow for the biosorbent dosage increments to improve biosorption. Therefore, pH can be considered as one of the dominant factors of the process. This conclusion confirms the results reviewed by Nguyen et al. [8]. As a general rule, they stated that as the pH solution is increased, so does the removal percentage of heavy metals. Similar to other biosorbents, the Fe-Sp used here seems to follow the trend that as pH values increase, the surface becomes more negatively charged which favors the metal ions uptake due to electrostatic interactions [8]. However, at pH values above seven, speciation such as $Pb(OH)^+$ and $Pb(OH)_2$ may occur which could lead to precipitation and subsequent overestimation of the removal percentage [63,64]. In practice, at pH values above seven it is difficult to distinguish between Pb precipitation and biosorption, therefore this limitation should be taken into consideration when determining the optimum biosorption conditions using modeling methodologies.

The pH_{pzc} value was determined as 3.2 and provided an important insight on the surface chemistry of the process (Fig. 7). At pH values below pH_{pzc} the biosorbent's surface acquired an overall positive charge that accounted for the low attraction—and therefore low removal—of the Pb^{2+} ions. As the pH of solution gradually increased and exceeded the pH_{pzc} value, Fe-Sp surface became negatively charged and the positive Pb^{2+} ions were increasingly attracted leading to higher removal %.

3.2.3.3. Interactive effect of pH and contact time. The critical pH effect can be also observed in Fig. 6(c), where the interaction between pH and contact time is shown. Even at the lowest contact time of 10 min, raising the pH from 2 to 8 resulted in a predicted biosorption increase of ~35% (from ~50 to 85%). At the optimum pH range of 6–7, increasing the contact time from 10 to 210 min, only increased biosorption from ~85 to ~95%. This is an indication of the fast kinetics of the process—even 10 min contact time was enough to remove ~85% of Pb^{2+} from solution. However, since removal efficiencies do not always reflect the true adsorption capacity of the adsorbent, it is more scientifically sound to compare adsorption capacities.

3.2.3.4. Interactive effect of contact time and biosorbent dose. The interaction between contact time and biosorbent dosage (Fig. 6(d)), confirmed that both these parameters did not show the critical effect pH had. At any single contact time, increasing the biosorbent dosage lead to only ~10% increase in predicted biosorption. Potentially higher biosorption would be expected if the biosorption mechanism depended
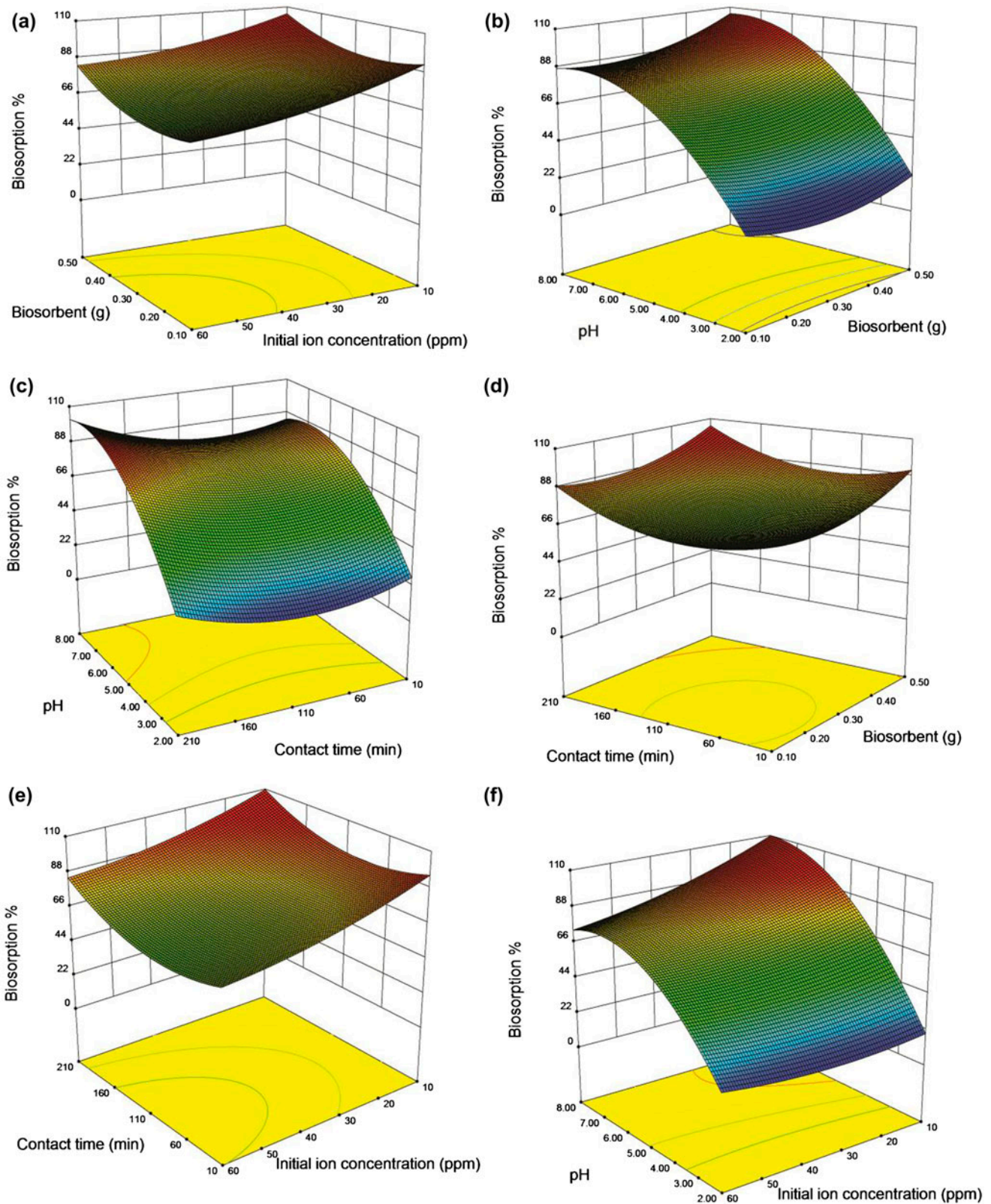
Fig. 6. 3-D surface plots for the interactive effect of (a) biosorbent dosage and initial Pb^{2+} concentration (pH 6, $t = 120$ min), (b) pH and biosorbent dosage ($C_{Pb} = 20$ ppm, $t = 120$ min), (c) pH and contact time (B. dose = 0.45 g, $C_{Pb} = 45$ ppm), (d) contact time and biosorbent dosage ($C_{Pb} = 45$ ppm, pH 6), (e) contact time and initial Pb^{2+} concentration (pH 6, B. dose = 0.30 g), and (f) pH and initial Pb^{2+} concentration (B. dose = 0.45 g, $t = 120$ min).
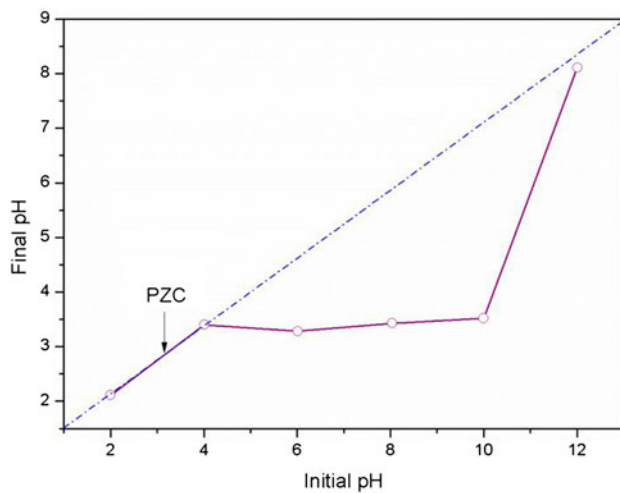
Fig. 7. Plot for the determination of pH_{pzc}.

solely on the surface area and/or the binding sites. However, at higher biosorbent doses, aggregation may occur, which leads to interferences between binding sites and a decrease in surface area [8,62]. At pH 6, a near-complete removal of Pb^{2+} was achieved at the highest biosorbent dosage (0.5 g) and contact time (210 min). This indicates that Fe-Sp can be used to remove Pb^{2+} in cases of slightly acidic industrial wastewaters. In such cases, wastewaters usually require an additional step of neutralization (liming) before heavy metal precipitation.

3.2.3.5. Interactive effect of contact time and initial metal concentration. At all combinations of contact time and initial metal concentration, biosorption percentage exceeded 80% (Fig. 6(e)). As shown earlier, changes in these parameters did not have a significant effect on Pb^{2+} removal. Increasing the initial metal concentration resulted in lower removal percentages. Given that adequate time was given for equilibrium (210 min), it can be assumed that Fe-Sp quickly became saturated, reached its adsorption capacity and a fraction of the increasing metal concentration remained in solution thereafter.

3.2.3.6. Interactive effect of pH and initial metal concentration. The predominant role of pH was again clear in Fig. 6(f), where pH was plotted against the initial Pb^{2+} concentration. However, it is interesting to note that Pb^{2+} concentration had practically no effect at pH 2, whereas at the optimum pH range of 6–7, increasing the metal concentration lead to a ~30% decrease in removal efficiency. Taking into account the reduction in removal efficiency also observed in Fig. 6(a) and (e)

when the initial Pb^{2+} concentration was raised, it appears that the adsorptive sites on the biosorbent surface gradually become saturated. This hypothesis is supported in the literature in cases of cadmium [65,66] and lead biosorption [67]. However, other works report the opposite trend, which they ascribed to a higher collision rate between the metal ions and the biosorbent surface [10]. More detailed investigations in a wider Pb^{2+} concentration range are required to safely conclude on this type of interaction.

The effects of all the independent variables (X_1, X_2, X_3, X_4) on biosorption are clearly shown on the perturbation plot (Fig. 8). The perturbation plot helps to compare the effect of all factors at a particular point in the design. The steep curvature of line B (pH) confirms the results discussed earlier, that pH is the predominant factor in biosorption of Pb^{2+}.

Using Eq. (6) and setting 80% as the minimum acceptable Pb^{2+} biosorption, the process was optimized within the following limits: biosorbent dosage range of 0.4–0.5 g, pH range of 5–8, contact time within 100–180 min, and initial Pb^{2+} concentration between 10 and 40 ppm. Within these boundaries, the optimum conditions were predicted as 0.5 g biosorbent, pH 6.75, 104 min contact time, and 25.42 ppm initial Pb^{2+} concentration, where 99.92 ± 4.6% metal biosorption could be achieved.
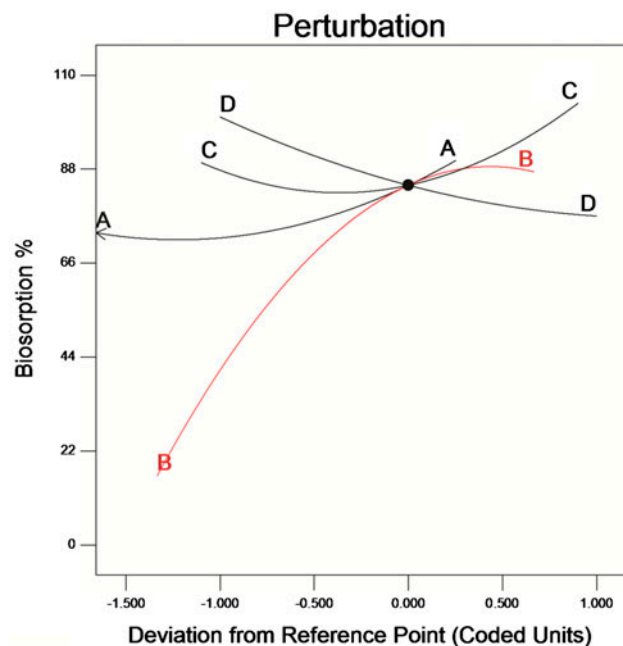

Fig. 8. Perturbation plot for biosorption Pb^{2+} using Fe-Sp (A: B. dose = 0.45 g, B: pH 6, C: time = 120 min, D: C_{Pb} = 35 ppm).

3.3. Biosorption equilibrium isotherms

The Pb^{2+}—biosorbent relationship at equilibrium was further investigated by fitting the experimental data on the Langmuir and Freundlich isotherm models. The Langmuir isotherm assumes monolayer adsorption onto a surface containing a specific number of adsorption sites and is described by the equation below:

$$\frac{C_e}{q_e} = \frac{1}{bq_{max}} + \frac{C_e}{q_{max}} \tag{10}$$

where q_e represents the quantity of metal adsorbed per amount of adsorbent at equilibrium (mg g^{-1}). The terms b and q_{max} are the adsorption binding constant and maximum adsorption capacity, respectively, and their values are obtained from the slope and interception of the plot.

The Freundlich isotherm is an empirical model that describes adsorption on the basis that surfaces consist of adsorption sites of varying affinities (heterogeneous). The experimental data were fitted in the logarithmic form of the Freundlich equation, shown below:

$$\ln q_e = \ln K_f - \frac{1}{n} \ln C_e \tag{11}$$

where K_f is a parameter reflecting the affinity of the adsorbate for the adsorbent, and $1/n$ is a dimensionless parameter reflecting heterogeneity. The higher the value of n, the greater the heterogeneity of the adsorbent. Both Langmuir and Freundlich isotherm parameters as well as a comparison with isotherm parameters obtained in other Pb^{2+} biosorption studies, are shown in Table 4.

The Freundlich isotherm model provided a considerably better fit for our data, compared to the Langmuir model (correlation coefficients of 0.994 and 0.947, respectively). This suggests biosorption on a heterogeneous, multi-layer surface. This is supported by the SEM results above, which show a heterogeneous Fe coating on the spore surface. Şener et al. [16] treated the same sporopollenin precursor with nitric acid and tested the modified biosorbent on Pb^{2+} removal from aqueous solutions. They reported a better fit of their data to the Langmuir model compared to the Freundlich model. Since the precursor and target metal ion is the same, the opposite result may be explained by the different treatment method, i.e. incomplete impregnation of sporopollenin with Fe_3O_4 particles, resulting in a non-uniform surface (see Section 3.1.2). The Langmuir isotherm indicated that the maximum Pb^{2+} uptake was 22.72 mg g^{-1} of Fe-Sp. The $1/n$ value was 0.863, indicating favorable biosorption of Pb^{2+}.

Table 4
Comparison of isotherm parameters obtained in this work to other Pb^{2+} sorption studies[a]

Langmuir parameters			Freundlich parameters				Refs.
q_{max} (mg g^{-1})	b (L mg^{-1})	R^2	K_f	n	R^2		
22.72	0.0047	0.947	9.15	1.15	0.994	Fe-modified sporopollenin	This work
nr[1]	0.0041	0.99	49	1.44	0.99	Modified sporopollenin	[21]
6.10	0.021	0.991	0.386	1.90	0.966	Pretreated sporopollenin	[16]
15.38	0.04	0.963	1.42	2.09	0.899	*Bacillus* sp. PZ-1	[64]
34.90	0.017	0.974	1.09	1.51	0.963	Yeast cells	[61]
116.69	0.023	0.991	4.27	1.49	0.989	Functionalized yeast cells	[61]
72.46	0.086	0.995	nr	nr	nr	Yeast cells	[68]
1.73	0.440	0.996	0.501	2.26	0.999	*Cocos nucifera* shell	[62]
3.40	0.368	0.959	0.879	1.40	0.998	*Moringa oleifera* seeds	[62]
125	0.022	0.996	2.664	1.11	0.995	Aquatic plant *Hydrilla verticillata*	[69]
55.55	0.58	0.999	20.94	2.09	0.991	*S. melongena* leave powder	[70]
238	0.014	0.971	10.4	1.78	0.992	*Sargassum ilicifolium* seaweed	[44]
0.103	0.236	0.968	48.23	5.263	0.996	Fungal strain *T. viride*	[48]
24.93	0.070	0.925	2.036	1.718	0.997	Hyacinth roots	[74]
91.74	0.109	0.941	8.366	1.331	0.998	Rice husk ash	[75]
83.33	0.051	0.974	3.82	1.44	0.994	Activated alumina	[76]
92.51	0.115	0.952	8.914	1.287	0.999	Oxygen furnace sludge	[77]
88.49	0.025	0.978	2.12	1.18	0.997	Sawdust	[78]
83.33	0.023	0.980	2.03	1.16	0.996	Neem bark	[78]

[a]This table is indicative and any comparisons are subject to additional variables such as the biosorbent surface area and initial pH of the metal solution.
Note: nr: not reported.

3.4. Adsorption kinetics

The removal of Pb^{2+} ions from the aqueous phase using sporopollenin was studied dynamically using kinetic models and examining the rate-controlling mechanism of the adsorption process such as chemisorption, diffusion control, and mass transfer. Mathematical models that are commonly applied to describe the kinetics of removal of metal ions are the pseudo-first-order (Lagergren's model), pseudo-second-order, and intra-particle diffusion kinetic models. To study the mechanism of Pb^{2+} adsorption process, the linearized equations of these kinetic models were applied and the results are shown in Fig. 9(a)–(c).

The pseudo-first-order kinetic model assumes a simple surface physical adsorption of the adsorbate and is described by the following equation:

$$\ln(q_e - q_t) = \ln(q_e) - k_A t \tag{12}$$

where q_e and q_t are the amounts of Pb^{2+} ions adsorbed on Fe-Sp (in mg(metal)/g(adsorbent)) at equilibrium and at time t, respectively, and k_A is the rate constant of the pseudo-first-order model for the adsorption (min^{-1}) [71]. The values of q_e and k_A can be obtained from the intercept and the slope of the linear plot of $\ln(q_e - q_t)$ against time (Fig. 9(a)).

If the adsorption mechanism followed a pseudo-second-order kinetics, then the rate limiting step would be chemical adsorption involving valency forces through sharing or exchange of electrons between the adsorbent and adsorbate. Pseudo-second-order kinetics are mathematically described by the following equation:

$$\frac{t}{q_t} = \frac{1}{k_B q_e^2} + \frac{t}{q_e} \tag{13}$$

where q_t and q_e are defined as above and k_B is the rate constant $(g\ mg^{-1}\ min^{-1})$. The slope and intercept of the linear plot of t/q against t determined the values of q_e and k_B, respectively (Fig. 9(b)).

The pseudo-first and second-order kinetic models do not adequately account for diffusion phenomena occurring during adsorption. The adsorption process may be controlled either pore diffusion, surface diffusion/adsorption on the pore surface, or a combination of these. The intra-particle diffusion model (IDM) is commonly used to describe the diffusion processes during adsorption of heavy metals by sorbents. It is described by the following equation:
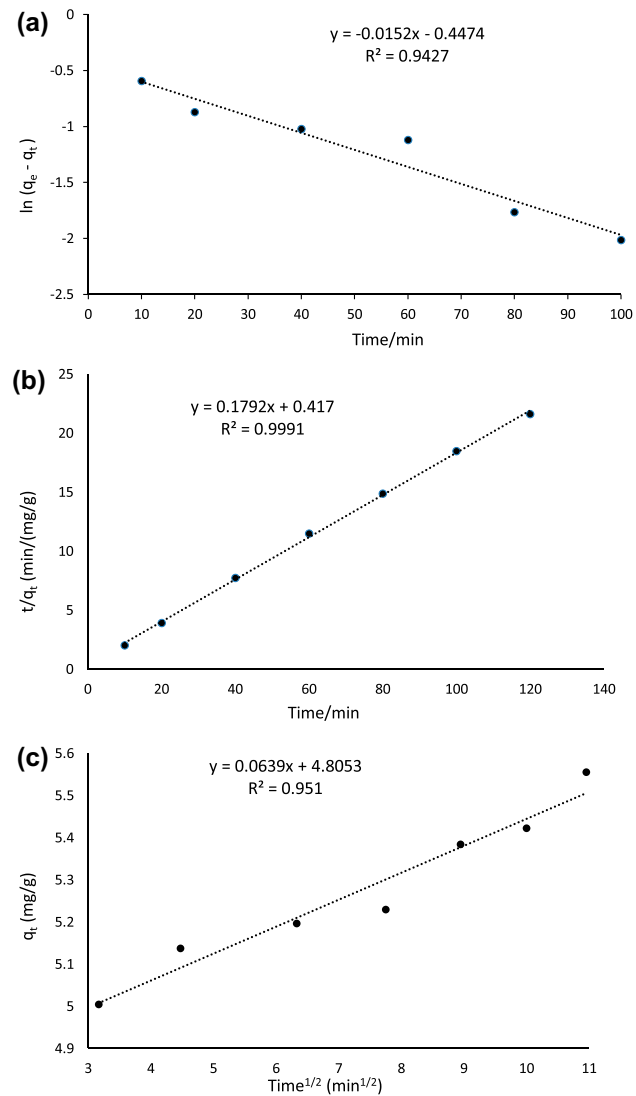
$$q_t = k_{int} t^{1/2} + C \tag{14}$$

Fig. 9. Linearized graphs of the pseudo-first (a), pseudo-second (b), and intra-particle diffusion model (c).

where C is the intercept and k_{int} is the intraparticle diffusion rate constant $(mg\ g^{-1}\ min^{-1/2})$, which can be evaluated from the slope of the linear plot of q_t vs. $t^{1/2}$ (Fig. 9(c)). If this plot is a straight line that goes through the origin of the axes, then the sorption process is exclusively controlled by intra-particle diffusion [72]. However, if the data exhibit multi-linear plots, then two or more steps influence the sorption process [73].

Table 5 presents the coefficients of the kinetic models. It can be seen that the pseudo-second-order regression coefficient (0.9991) is considerably higher compared to the pseudo-first-order (0.9427) and the intra-particle diffusion (0.951) coefficients. Additionally, the calculated q value for the pseudo-second-order model closely agrees with the experimental q value, contrary to the calculated q value for the

Table 5
Parameters of the pseudo-first-order, pseudo-second-order, and intra-particle diffusion models

Kinetic model	Parameter	Value
Pseudo-first-order	$q_{e,experimental}$ (mg g^{-1})	5.556
	$q_{e,calculated}$ (mg g^{-1})	0.639
	k_A (min^{-1})	0.0152
	R^2	0.9427
Pseudo-second-order	$q_{e,experimental}$ (mg g^{-1})	5.556
	$q_{e,calculated}$ (mg g^{-1})	5.58
	k_B (g mg^{-1} min^{-1})	0.076
	R^2	0.9991
Intra-particle diffusion	k_{int} (mg g^{-1} min$^{-1/2}$)	0.0639
	C (mg g^{-1})	4.8
	R^2	0.951

pseudo-first-order model. Therefore, we can safely assume that Pb^{2+} adsorption on Fe-Sp follows the pseudo-second-order kinetic model and chemisorption is the rate-limiting step. This conclusion agrees with previous adsorption studies of Pb^{2+} on various biomasses [33,62]. The high value for C in the intra-particle diffusion plot may be attributed to considerable differences in mass transfer in the initial and final stages of Pb^{2+} biosorption [62].

4. Conclusions

Fe-Sp was synthesized and tested as a novel biosorbent for removal of Pb^{2+} from aqueous solution. Biosorption efficiency was optimized by the application of the Box–Behnken experimental design in combination with RSM. It was determined that pH was the dominant factor of the process, whereas biosorbent dosage, contact time, and Pb^{2+} concentration had a reduced effect within the system boundaries. The optimized values for biosorbent dosage, pH, contact time, and initial Pb^{2+} concentration were 0.5 g, 6.75, 104 min, and 25.42 ppm, respectively. At these conditions, the removal percentage for Pb^{2+} was predicted to be 99.92 ± 4.6%. Equilibrium studies were performed by using isotherm models and it was determined that the Freundlich model provided a better fit for the experimental data. The maximum biosorption capacity obtained from the Langmuir isotherm model was 22.72 mg g^{-1}. The kinetics of the process followed a pseudo-second-order model. Overall, Fe-Sp showed a positive behavior as biosorbent. Compared to other magnetically or otherwise modified biosorbents, Fe-Sp exhibited comparable adsorption capacities (Table 4). From a technical point of view, the biosorbent could

be easily collected and removed from solution using a magnetic field, thus reducing unnecessary post-treatment steps and costs.

More work is required toward establishing Fe-Sp as an effective biosorbent for a wide range of metals. Real industrial wastewaters often contain several heavy metals, some of which may compete with Pb^{2+} for active adsorption sites on the biosorbent. This would result in lower removal efficiency for Pb^{2+} and an overall decreased performance for the biosorbent. Any optimization would need to take into consideration the number of heavy metals, their concentrations, and the interactions between them and with the biosorbent surface.

References

[1] M. Jaishankar, T. Tseten, N. Anbalagan, B.B. Mathew, K.N. Beeregowda, Toxicity, mechanism and health effects of some heavy metals, Interdiscip. Toxicol. 7 (2014) 60–72.
[2] G. Flora, D. Gupta, A. Tiwari, Toxicity of lead: A review with recent updates, Interdiscip. Toxicol. 5 (2012) 47–58.
[3] A.M. Showkat, Y.P. Zhang, S.K. Min, A.I. Gopalan, K.R. Reddy, K.P. Lee, Analysis of heavy metal toxic ions by adsorption onto amino-functionalized ordered mesoporous silica, Bull. Korean Chem. Soc. 28 (2007) 1985–1992.
[4] P. Hadi, M.-H. To, C.-W. Hui, C.S.K. Lin, G. McKay, Aqueous mercury adsorption by activated carbons, Water Res. 73 (2015) 37–55.
[5] F. Fu, Q. Wang, Removal of heavy metal ions from wastewaters: A review, J. Environ. Manage. 92 (2011) 407–418.
[6] A. Mudhoo, V.K. Garg, S. Wang, Removal of heavy metals by biosorption, Environ. Chem. Lett. 10 (2012) 109–117.
[7] I. Michalak, K. Chojnacka, A. Witek-Krowiak, State of the art for the biosorption process—A review, Appl. Biochem. Biotechnol. 170 (2013) 1389–1416.
[8] T.A.H. Nguyen, H.H. Ngo, W.S. Guo, J. Zhang, S. Liang, Q.Y. Yue, Q. Li, T.V. Nguyen, Applicability of agricultural waste and by-products for adsorptive removal of heavy metals from wastewater, Bioresour. Technol. 148 (2013) 574–585.
[9] R.K. Gautam, A. Mudhoo, G. Lofrano, M.C. Chattopadhyaya, Biomass-derived biosorbents for metal ions sequestration: Adsorbent modification and activation methods and adsorbent regeneration, J. Environ. Chem. Eng. 2 (2014) 239–259.

[10] J. Wang, C. Chen, Chitosan-based biosorbents: Modification and application for biosorption of heavy metals and radionuclides, Bioresour. Technol. 160 (2014) 129–141.

[11] A.A. Dobritsa, J. Shrestha, M. Morant, F. Pinot, M. Matsuno, R. Swanson, B.L. Moller, D. Preuss, CYP704B1 is a long-chain fatty acid omega-hydroxylase essential for sporopollenin synthesis in pollen of Arabidopsis, Plant Physiol. 151 (2009) 574–589.

[12] S.J. Archibald, S.L. Atkin, W. Bras, A. Diego-Taboada, G. Mackenzie, J.F.W. Mosselmans, S. Nikitenko, P.D. Quinn, M.F. Thomas, N.A. Young, How does iron interact with sporopollenin exine capsules? An X-ray absorption study including microfocus XANES and XRF imaging, J. Mater. Chem. B 2 (2014) 945–959.

[13] F. Gode, E. Pehlivan, Sorption of Cr(III) onto chelating b-DAEG-sporopollenin and CEP-sporopollenin resins, Bioresour. Technol. 98 (2007) 904–911.

[14] I.H. Gubbuk, Isotherms and thermodynamics for the sorption of heavy metal ions onto functionalized sporopollenin, J. Hazard. Mater. 186 (2011) 416–422.

[15] S. Sayin, I.H. Gubbuk, M. Yilmaz, Preparation of calix [4]arene-based sporopollenin and examination of its dichromate sorption ability, J. Inclusion Phenom. Macrocyclic Chem. 75 (2013) 111–118.

[16] M. Şener, D.H.K. Reddy, B. Kayan, Biosorption properties of pretreated sporopollenin biomass for lead(II) and copper(II): Application of response surface methodology, Ecol. Eng. 68 (2014) 200–208.

[17] İ. Sargın, G. Arslan, Chitosan/sporopollenin microcapsules: Preparation, characterisation and application in heavy metal removal, Int. J. Biol. Macromol. 75 (2015) 230–238.

[18] M.A. Kamboh, M. Yilmaz, Synthesis of N-methylglucamine functionalized calix[4]arene based magnetic sporopollenin for the removal of boron from aqueous environment, Desalination 310 (2013) 67–74.

[19] M. Sahin, I.H. Gubbuk, N. Kocak, Synthesis and characterization of sporopollenin-supported schiff bases and ruthenium(III) sorption studies, J. Inorg. Organomet. Polym Mater. 22 (2012) 1279–1286.

[20] N. Kocak, M. Sahin, I.H. Gubbuk, Synthesized of sporopollenin-immobilized schiff bases and their vanadium(IV) sorption studies, J. Inorg. Organomet. Polym Mater. 22 (2012) 852–859.

[21] I.H. Gubbuk, L. Gürfidan, S. Erdemir, M. Yilmaz, Surface modification of sporopollenin with calixarene derivative, Water Air Soil Pollut. 223 (2012) 2623–2632.

[22] I.H. Gubbuk, M. Ozmen, E. Maltas, Immobilization and characterization of hemoglobin on modified sporopollenin surfaces, Int. J. Biol. Macromol. 50 (2012) 1346–1352.

[23] K.R. Reddy, K.-P. Lee, A.I. Gopalan, M.S. Kim, A.M. Showkat, Y.C. Nho, Synthesis of metal (Fe or Pd)/alloy (Fe–Pd)-nanoparticles-embedded multiwall carbon nanotube/sulfonated polyaniline composites by γ irradiation, J. Polym. Sci. Part A: Polym. Chem. 44 (2006) 3355–3364.

[24] K.R. Reddy, K.P. Lee, A.I. Gopalan, Self-assembly approach for the synthesis of electro-magnetic functionalized Fe₃O₄/polyaniline nanocomposites: Effect of dopant on the properties, Colloids Surf. A 320 (2008) 49–56.

[25] K.R. Reddy, K.-P. Lee, J.Y. Kim, Y. Lee, Self-assembly and graft polymerization route to monodispersed Fe3O4@SiO2—Polyaniline core-shell composite nanoparticles: Physical properties, J. Nanosci. Nanotechnol. 8(11) (2008) 5632–5639.

[26] K.R. Reddy, W. Park, B.C. Sin, J. Noh, Y. Lee, Synthesis of electrically conductive and superparamagnetic monodispersed iron oxide-conjugated polymer composite nanoparticles by in situ chemical oxidative polymerization, J. Colloid Interface Sci. 335 (2009) 34–39.

[27] K.P. Reddy, K. Nakata, T. Ochiai, T. Murakami, D.A. Tryk, A. Fujishima, Nanofibrous TiO₂-Core/conjugated polymer-sheath composites: Synthesis, J. Nanosci. Nanotechnol. 10(12) (2010) 7951–7957.

[28] K.R. Reddy, V.G. Gomes, M. Hassan, Carbon functionalized TiO₂ nanofibers for high efficiency photocatalysis, Mater. Res. Express 1 (2014) 1–12, 015012.

[29] M. Kishimoto, M. Minagawa, H. Yanagihara, T. Oda, N. Ohkochi, E. Kita, Synthesis and magnetic properties of platelet γ-Fe₂O₃ particles for medical applications using hysteresis-loss heating, J. Magn. Magn. Mater. 324 (2012) 1285–1289.

[30] G.-R. Xu, J.-N. Wang, C.-J. Li, A new strategy for the synthesis of iron-oxide nanocrystals by using a single-spinneret electrospinning technique, Chem. Asian J. 8 (10) 2013 2453–2458.

[31] G. Hong, X. Li, L. Shen, M. Wang, C. Wang, X. Yu, X. Wang, High recovery of lead ions from aminated polyacrylonitrile nanofibrous affinity membranes with micro/nano structure, J. Hazard. Mater. 295 (2015) 161–169.

[32] Y. Hwang, P.D. Mines, M.H. Jakobsen, H.R. Andersen, Simple colorimetric assay for dehalogenation reactivity of nanoscale zero-valent iron using 4-chlorophenol, Appl. Catal. B 166–167 (2015) 18–24.

[33] R. Sivashankar, A.B. Sathya, K. Vasantharaj, V. Sivasubramanian, Magnetic composite an environmental super adsorbent for dye sequestration—A review. Environ. Nanotechnol. Monit. Manage. 1–2 (2014) 36–49.

[34] T. Mayo, C.T. Yavuz, S. Yean, L. Cong, W.W. Yu, J. Falkner, A. Kan, M. Tomson, V.L. Colvin, The effect of nanocrystalline magnetite size on arsenic removal, Sci. Technol. Adv. Mater. 8 (2006) 71–75.

[35] V. Sureshkumar, S.C.G. Kiruba Daniel, K. Ruckmani, M. Sivakumar, Fabrication of chitosan–magnetite nanocomposite strip for chromium removal, Appl. Nanosci. 6 (2015) 277–285.

[36] I. Safarik, K. Horska, B. Svobodova, M. Safarikova, Magnetically modified spent coffee grounds for dyes removal, Eur. Food Res. Technol. 234 (2012) 345–350.

[37] E. Baldikova, M. Safarikova, I. Safarik, Organic dyes removal using magnetically modified rye straw, J. Magn. Magn. Mater. 380 (2015) 181–185.

[38] H. Yavuz, A. Denizli, H. Güngüneş, M. Safarikova, I. Safarik, Biosorption of mercury on magnetically modified yeast cells, Sep. Purif. Technol. 52 (2006) 253–260.

[39] M.E. Mahmoud, S.B. Ahmed, M.M. Osman, T.M. Abdel-Fattah, A novel composite of nanomagnetite-immobilized-baker's yeast on the surface of activated carbon for magnetic solid phase extraction of Hg(II), Fuel 139 (2015) 614–621.

[40] T.M. Abdel-Fattah, M.E. Mahmoud, M.M. Osmam, S.B. Ahmed, Magnetically active biosorbent for chromium species removal from aqueous media, J. Environ. Sci. Health Part A 49 (2014) 1064–1076.

[41] H. Wang, Y. Ji, Q. Tian, K. Horska, X. Shao, Z. Maderova, X. Miao, M. Safarikova, I. Safarik, Biosorption of uranium by magnetically modified wheat bran, Sep. Sci. Technol. 49 (2014) 2534–2539.

[42] M. Sarkar, P. Majumdar, Application of response surface methodology for optimization of heavy metal biosorption using surfactant modified chitosan bead, Chem. Eng. J. 175 (2011) 376–387.

[43] K. Deng, P. Yin, X. Liu, Q. Tang, R. Qu, Modeling, analysis and optimization of adsorption parameters of Au(III) using low-cost agricultural residuals buckwheat hulls, J. Ind. Eng. Chem. 20 (2014) 2428–2438.

[44] R. Tabaraki, A. Nateghi, S. Ahmady-Asbchin, Biosorption of lead (II) ions on *Sargassum ilicifolium*: Application of response surface methodology, Int. Biodeterior. Biodegrad. 93 (2014) 145–152.

[45] L. Fan, C. Luo, Z. Lv, F. Lu, H. Qiu, Preparation of magnetic modified chitosan and adsorption of Zn^{2+} from aqueous solutions, Colloids Surf. B 88 (2011) 574–581.

[46] C. Yuwei, W. Jianlong, Preparation and characterization of magnetic chitosan nanoparticles and its application for Cu(II) removal, Chem. Eng. J. 168 (2011) 286–292.

[47] G. Newcombe, R. Hayes, M. Drikas, Granular activated carbon: Importance of surface properties in the adsorption of naturally occurring organics, Colloids Surf. A 78 (1993) 65–71.

[48] R. Singh, R. Chadetrik, R. Kumar, K. Bishnoi, D. Bhatia, A. Kumar, N.R. Bishnoi, N. Singh, Biosorption optimization of lead(II), cadmium(II) and copper(II) using response surface methodology and applicability in isotherms and thermodynamics modeling, J. Hazard. Mater. 174 (2010) 623–634.

[49] M. Cobas, M.A. Sanromán, M. Pazos, Box–Behnken methodology for Cr(VI) and leather dyes removal by an eco-friendly biosorbent: F. vesiculosus, Bioresour. Technol. 160 (2014) 166–174.

[50] D. Das, R. Vimala, N. Das, Biosorption of Zn(II) onto *Pleurotus platypus*: 5-Level Box–Behnken design, equilibrium, kinetic and regeneration studies, Ecol. Eng. 64 (2014) 136–141.

[51] S.S. Melvin, A.A.M. Evy, R. Chidambaram, Isotherm modelling, kinetic study and optimization of batch parameters using response surface methodology for effective removal of Cr(VI) using fungal biomass, PLoS ONE 10 (2015) 1–15, Article Number: e0116884.

[52] C.J.S. Varshini, D. Das, N. Das, Optimization of parameters for praseodymium(III) biosorption onto biowaste materials using response surface methodology: Equilibrium, kinetic and regeneration studies, Ecol. Eng. 81 (2015) 321–327.

[53] S.L.C. Ferreira, R.E. Bruns, H.S. Ferreira, G.D. Matos, J.M. David, G.C. Brandão, E.G.P. da Silva, L.A. Portugal, P.S. dos Reis, A.S. Souza, W.N.L. dos Santos, Box–Behnken design: An alternative for the optimization of analytical methods, Anal. Chim. Acta 597 (2007) 179–186.

[54] K. Yetilmezsoy, S. Demirel, R.J. Vanderbei, Response surface modeling of Pb(II) removal from aqueous solution by *Pistacia vera* L.: Box–Behnken experimental design, J. Hazard. Mater. 171 (2009) 551–562.

[55] B. Kayan, B. Gözmen, Degradation of Acid Red 274 using H_2O_2 in subcritical water: Application of response surface methodology, J. Hazard. Mater. 201–202 (2012) 100–106.

[56] S.S. Moghaddam, M.R.A. Moghaddam, M. Arami, Coagulation/flocculation process for dye removal using sludge from water treatment plant: Optimization through response surface methodology, J. Hazard. Mater. 175 (2010) 651–657.

[57] S. Wilmesmeier, S. Steuernagel, R. Wiermann, Comparative FTIR and ^{13}C CP/MAS NMR spectroscopic investigations on sporopollenin of different systematic origins, Z. Naturforsch. 48c (1993) 697–701

[58] W.T. Fraser, A.C. Scott, A.E.S. Forbes, I.J. Glasspool, R.E. Plotnick, F. Kenig, B.H. Lomax, Evolutionary stasis of sporopollenin biochemistry revealed by unaltered Pennsylvanian spores, New Phytol. 196 (2012) 397–401.

[59] K.P. Singh, S. Gupta, A.K. Singh, S. Sinha, Optimizing adsorption of crystal violet dye from water by magnetic nanocomposite using response surface modeling approach, J. Hazard. Mater. 186 (2011) 1462–1473.

[60] B. Gözmen, O. Sonmez, M. Turabik, Response surface methodology for oxidation degradation of the Basic Yellow 28 dye by temperature and ferrous ion activated persulfate, Asian J. Chem. 25 (2013) 6831–6839.

[61] X. Ma, W. Cui, L. Yang, Y. Yang, H. Chen, K. Wang, Efficient biosorption of lead(II) and cadmium(II) ions from aqueous solutions by functionalized cell with intracellular $CaCO_3$ mineral scaffolds, Bioresour. Technol. 185 (2015) 70–78.

[62] M.A. Acheampong, E.D.O. Ansa, M.Y. Woode, E. Awuah, Biosorption of Pb(II) onto cocos nucifera shell and moringa oleifera seeds, Chem. Eng. Commun. 202 (2015) 946–953.

[63] A. Choi, S. Wang, M. Lee, Biosorption of cadmium, copper, and lead ions from aqueous solutions by *Ralstonia* sp. and *Bacillus* sp. isolated from diesel and heavy metal contaminated soil, Geosci. J. 13 (2009) 331–341.

[64] G. Ren, Y. Jin, C. Zhang, H. Gu, J. Qu, Characteristics of *Bacillus* sp. PZ-1 and its biosorption to Pb(II), Ecotoxicol. Environ. Saf. 117 (2015) 141–148.

[65] N. Kannan, T. Veemaraj, Detoxification of toxic metal ions by sorption onto activated carbon from *Hevea Brasiliensis* bark—A Comparative study, Global NEST J. 12(2) (2010) 197–205.

[66] P.S. Kumar, S. Ramalingam, V. Sathyaselvabala, S.D. Kirupha, A. Murugesan, S. Sivanesan, Removal of cadmium(II) from aqueous solution by agricultural waste cashew nut shell, Korean J. Chem. Eng. 29(6) (2012) 756–768.

[67] M.A. Ashraf, M.J. Maah, I. Yusoff, Removal of lead from synthetic solutions by protonated teleosts biomass, E-J. Chem. 9(1) (2012) 345–353.

[68] S. Amirnia, M.B. Ray, A. Margaritis, Heavy metals removal from aqueous solutions using *Saccharomyces cerevisiae* in a novel continuous bioreactor-bioorption system, Chem. Eng. J. 264 (2015) 863–872.

[69] P.K.D. Chathuranga, D.M.R.E.A. Dissanayake, N. Priyantha, S.S. Iqbal, M.C.M. Iqbal, Biosorption and desorption of lead(II) by *hydrilla verticillata*, Biorem. J. 18 (2014) 192–203.

[70] G. Yuvaraja, N. Krishnaiah, M.V. Subbaiah, A. Krishnaiah, Biosorption of Pb(II) from aqueous solution by *Solanum melongena* leaf powder as a low-cost biosorbent prepared from agricultural waste, Colloids Surf. B 114 (2014) 75–81.

[71] A.A. Farghali, M. Bahgat, A. Enaiet Allah, M.H. Khedr, Adsorption of Pb(II) ions from aqueous solutions using copper oxide nanostructures, Beni-Suef Univ., J. Basic Appl. Sci. 2 (2013) 61–71.

[72] W.J. Weber, J.C. Morris, Kinetics of adsorption on carbon from solution, J. Sanit. Eng. Div. ASCE 89 (1963) 31–59.

[73] V. Fierro, V. Torné-Fernández, D. Montané, A. Celzard, Adsorption of phenol onto activated carbons having different textural and surface properties, Microporous Mesoporous Mater. 111 (2008) 276–284.

[74] B. Singha, S.K. Das, Removal of Pb(II) ions from aqueous solution and industrial effluent using natural biosorbents, Environ. Sci. Pollut. Res. 19 (2012) 2212–2226.

[75] T.K. Naiya, A.K. Bhattacharya, S. Mandal, S.K. Das, The sorption of lead(II) ions on rice husk ash, J. Hazard. Mater. 163 (2009) 1254–1264.

[76] T.K. Naiya, A.K. Bhattacharya, S.K. Das, Adsorption of Cd(II) and Pb(II) from aqueous solutions on activated alumina, J. Colloid Interface Sci. 333 (2009) 14–26.

[77] T.K. Naiya, A.K. Bhattacharya, S.K. Das, Clarified sludge (basic oxygen furnace sludge)—An adsorbent for removal of Pb(II) from aqueous solutions—Kinetics, thermodynamics and desorption studies, J. Hazard. Mater. 170 (2009) 252–262.

[78] T.K. Naiya, A.K. Bhattacharya, S.K. Das, Adsorption of Pb(II) by sawdust and neem bark from aqueous solutions, Environ. Prog. Sustain. Energy 27 (2008) 313–328.